



HAL
open science

Fatigue of natural rubber under different temperatures

Benoît Ruellan, Jean-Benoit Le Cam, I. Jeanneau, F. Canevet, F. Mortier,
Eric Robin

► **To cite this version:**

Benoît Ruellan, Jean-Benoit Le Cam, I. Jeanneau, F. Canevet, F. Mortier, et al.. Fatigue of natural rubber under different temperatures. *International Journal of Fatigue*, 2019, 124, pp.544-557. 10.1016/j.ijfatigue.2018.10.009 . hal-02121501

HAL Id: hal-02121501

<https://univ-rennes.hal.science/hal-02121501>

Submitted on 7 May 2020

HAL is a multi-disciplinary open access archive for the deposit and dissemination of scientific research documents, whether they are published or not. The documents may come from teaching and research institutions in France or abroad, or from public or private research centers.

L'archive ouverte pluridisciplinaire **HAL**, est destinée au dépôt et à la diffusion de documents scientifiques de niveau recherche, publiés ou non, émanant des établissements d'enseignement et de recherche français ou étrangers, des laboratoires publics ou privés.

Fatigue of natural rubber under different temperatures

B. Ruellan^{a,b,c}, J.-B. Le Cam^{a,c,1}, I. Jeanneau^{b,c}, F. Canévet^{b,c},
F. Mortier^{b,c}, E. Robin^{a,c}

^a*Université de Rennes 1, Institut de Physique UMR 6251 CNRS/Université de Rennes 1, Campus de Beaulieu, Bât. 10B, 35042 Rennes Cedex, France.*

^b*Cooper Standard, 194 route de Lorient, 35043 Rennes-France.*

^c*LC-DRIME, Joint Research Laboratory, Cooper Standard-Institut de Physique UMR 6251, Campus de Beaulieu, Bât. 10B, 35042 Rennes Cedex, France.*

Abstract

Natural rubbers have extraordinary physical properties, typically the ability to crystallize under tension. Especially, they exhibit a high fatigue resistance. Furthermore, strain-induced crystallization (SIC) is a high thermo-sensitive phenomenon. Better understanding how SIC reinforces fatigue life and how temperature affects this property is therefore a key point to improve the durability of rubbers. The present study investigates temperature effects on the fatigue life reinforcement due to SIC for non-relaxing loadings. After a brief state of the art that highlights a lack of experimental results in this field, a fatigue test campaign has been defined and was carried out. Results obtained at 23°C were first described at the macroscopic scale. Both damage modes and number of cycles at crack initiation were mapped in the Haigh diagram. Fatigue damage mechanisms were then investigated at the microscopic scale, where the signature of SIC reinforcement in the crack growth mechanisms has been identified. Typically, fatigue striations, wrenchings and cones peopled the fracture surfaces obtained under non-relaxing loading conditions. At 90°C, fatigue life reinforcement was still observed. It is lower than at 23°C. Only one damage mode was observed at the macroscopic scale. At the microscopic scale, fracture surfaces looked like the ones of non-crystallizable rubbers. At 110°C, the fatigue life reinforcement totally disappeared.

Key words: natural rubber, fatigue, lifetime reinforcement, temperature effects, strain-induced crystallization

1 Introduction

Fatigue of crystallizable rubbers has been widely investigated since the pioneer work by Cadwell *et al.* (1940). This study revealed the significant influence of the mean strain on natural rubber (NR) lifetime: for non-relaxing loading conditions (*i.e.* $R_\varepsilon > 0$)², a strong lifetime reinforcement was observed and attributed to strain-induced crystallization (SIC). On an industrial point of view, filled NR is a good candidate for anti-vibratory parts thanks to its ability to resist crack propagation. Even though anti-vibratory parts undergo temperature up to 110°C in the engine environment, only few studies investigated the effect of temperature on the lifetime reinforcement, while SIC exhibits a high thermosensitivity (Fielding, 1943; Lindley, 1974; Bathias *et al.*, 1998; Le Chenadec, 2008). Better understanding how SIC reinforces fatigue life and how temperature affects this property is a key point to improve the durability of rubbers. The present study investigates how temperature affects the deformation mechanisms, particularly the ability of NR to crystallize under strain for non-relaxing loading conditions.

The paper is composed of two parts. The first one is a state of the art on fatigue of rubber. Tests performed, fatigue life criteria and diagrams used to represent the results are described. The effects of non-relaxing loading conditions and of the test temperature on the fatigue life reinforcement of natural rubber are presented. This state of the art clearly points out the reason why new fatigue tests are required. The second part of the paper presents the fatigue tests carried out. The experimental setup, the sample geometry, the material and the fatigue tests are described. Results are summed up from the Haigh diagram. The fatigue behavior of the material is then presented at 90 and 110°C. Finally, a discussion on the effect of the temperature on the reinforcement due to SIC for non-relaxing loading is proposed.

2 State of the art

Literature on fatigue behavior of elastomers is abundant. Two approaches are classically distinguished, namely the crack initiation and the crack propagation approaches (Mars and Fatemi, 2002). In the present state of the art, only the former is addressed. Even though studies differed in the sample geometries tested,

¹ Corresponding author jean-benoit.lecam@univ-rennes1.fr Fax : (+33) 223 236 111

² R_ε is the loading ratio, defined as $\frac{\varepsilon_{min}}{\varepsilon_{max}}$

in the material formulations and in the loading conditions, general comments can be drawn on the effect of the loading condition, of the temperature, and on the damage mechanisms.

2.1 Experiments carried out

2.1.1 Sample geometry and materials

Volumetric samples were generally preferred to plane samples because they are more representative of rubber parts. Plane samples were classically used to investigate crack growth (Greensmith and Thomas, 1956; Greensmith, 1956; Lake and Lindley, 1964; Lindley, 1974; Lake, 1995; Bathias *et al.*, 1997). Cadwell *et al.* (1940) initially used cylindrical samples, which were replaced by a Diabolo-like geometry in the work by Beatty (1964). This type of geometry was then used as the reference one (Svensson, 1981; Lu, 1991; Xie, 1992; Bathias *et al.*, 1998; André *et al.*, 1999; Robisson, 2000; Saintier, 2000; Kim *et al.*, 2004; Ostoja-Kuczynski *et al.*, 2003; Le Cam, 2005; Raoult, 2005; Bennani, 2006; Oshima *et al.*, 2007; Le Cam *et al.*, 2008, 2013; Woo *et al.*, 2009; Ayoub, 2010; Moon *et al.*, 2011; Flamm *et al.*, 2011; Poisson, 2012; Wang *et al.*, 2014; Shangguan *et al.*, 2017; Neuhaus *et al.*, 2017). Such geometry is well adapted to fatigue since no buckling is induced under compression and fatigue damage generally occurs at the surface of the sample, at half of its height, due to stress and strain concentration. Other sample geometries, AE2 and AE5 with lower radius of curvature (2 and 5 mm, respectively), were introduced and used for investigating multiaxial fatigue of rubber (André *et al.*, 1999; Robisson, 2000; Saintier, 2000; Ostoja-Kuczynski, 2005; Le Cam, 2005; Ayoub, 2010). The materials considered in the literature were mainly filled NR.

2.1.2 Loading conditions

Cadwell *et al.* (1940) investigated the effect of the displacement amplitude at a fixed minimum of displacement and the effect of the minimum displacement at a fixed displacement amplitude, for displacement prescribed tests on carbon black filled NR cylindrical samples. The following studies aimed at distinguishing the fatigue response of crystallizable rubbers from non-crystallizable ones (Fielding, 1943; Beatty, 1964). Considering multiaxial fatigue, the first studies were provided by Roberts and Benzies (1977) and Svensson (1981). They investigated the effect of biaxiality on plane samples and the effect of shear at prescribed displacement with preloading on Diabolo samples, respectively. Later, more complex loading were used. André *et al.* (1999) extended their uni-axial study of a filled NR to

torsion, tension-compression and tension-tension carried out with AE2 samples. In a comparable approach, Robisson (2000) studied silica filled SBR under torsion and Saintier (2000) investigated tension-compression with and without a torsion preloading using Diabolo, AE2 and AE5 samples. Ostoja-Kuczynski (2005) also carried out fatigue tests with Diabolo and AE2 samples under tension-compression, relaxing tension, tension-tension, relaxing torsion, fully reversed torsion and relaxing tension-torsion in opposite phases³.

The most exhaustive fatigue campaign was carried out by Mars (2001). The author used an annular sample tested in repeated tension ($R_U = 0$) prescribed under displacement and torsion prescribed under angle ($R_\theta = 0$ and -1) before combining in-phase and out-of-phase tension-torsion. Ayoub (2010) carried out similar tests on diabolo samples. Note that temperature was mainly investigated through fatigue tests carried out at constant loading ratios (Lu, 1991; Xie, 1992; Duan *et al.*, 2016). Nevertheless Bathias *et al.* (1998) investigated the effect of the stress amplitude on different elastomers (namely NR, CR and SBR) at 25, 50 and 80°C on diabolo sample tested under prescribed force.⁴ Le Chenadec (2008) investigated the fatigue behavior of a filled NR tested at $R_\epsilon = 0$, for different ϵ_{max} and different R_ϵ at a given ϵ_{max} for several temperatures from 5 to 100°C. Note that in this study, the temperature considered is the one measured at the sample surface, in order to take self-heating into account. Considering frequencies applied, they were generally chosen to optimize the trade-off between heat built-up and fatigue tests duration. It corresponded to frequencies ranging from 0.5 to several Hertz.

2.1.3 End-of-life criterion

Considering the crack initiation approach applied on volumetric samples, four criteria were used to determine the end-of-life:

- (i) the sample failure (Cadwell *et al.*, 1940; Kim *et al.*, 2004; Poisson, 2012; Wang *et al.*, 2014);
- (ii) the apparition of a crack of a critical length at the sample surface. The crack length varied depending on the authors: 1 mm for Robisson (2000); Saintier (2000); Bennani (2006); Ayoub (2010), between 1 and 2.5 mm for Svensson (1981), 3 mm for Xie (1992) and André *et al.* (1999). The choice of a crack length

³ these fatigue tests are presented in Le Cam *et al.* (2013)

⁴ In this study, the authors did not provide if the fatigue tests were performed under prescribed displacement or force. They stated that they investigated the effect of the mean stress, which seems to indicate that tests were performed under prescribed force (as the material is viscoelastic).

- is not physically motivated and purely conventional as discussed in (André *et al.*, 1999). This criterion is based on an optical observation that is difficult to perform and does not apply to internal crack initiation;
- (iii) a critical value of a macroscopic parameter. It applies for initiation of external as well as internal cracks and is therefore easily applicable to fatigue tests. Authors linked the sample end-of-life to a loss of the chosen parameter: 15% of the maximal force at the 128th cycle (Mars, 2001), 50% of the stabilized shearing effort (Xie, 1992), 20% of the first cycle effort (Woo *et al.*, 2009; Moon *et al.*, 2011; Shangguan *et al.*, 2017), 20% of the maximal displacement at the 1000th cycle for tests under prescribed force (Neuhaus *et al.*, 2017);
 - (iv) the brutal decrease of the maximal reaction force (Lu, 1991; Xie, 1992), it was later formalized by Ostoja-Kuczynski *et al.* (2003) as the number of cycles at which the derivative of the stiffness is not constant anymore (Le Chenadec, 2008; Le Saux, 2010; Masquelier, 2014). In practice, this number of cycles is correlated with the occurrence of a few mm long crack at the sample surface (2 mm for Ostoja-Kuczynski (2005) and Le Cam (2005)).

Since end-of-life criteria differed from one study to another, comparing quantitatively fatigue data from studies available in the literature is complicated.

2.1.4 Representation used and the question of the damage predictor

Two types of lifetime representation are reported in the literature, both derive from studies on fatigue of metals: Stress-Number of cycles (S-N) curves and the Haigh diagram.

(i) Classically, S-N curves (also named Wöhler curves) were used to investigate fatigue of metallic materials (Wöhler, 1860). In this case, the stress is chosen as the relevant quantity. S-N curves have been used to describe the fatigue behavior of elastomers with different quantities: the maximum stress σ_{max} (Lu, 1991; Abraham *et al.*, 2005), the mean stress σ_{mean} (Bathias *et al.*, 1998), the maximum strain ε_{max} (Lu, 1991; Xie, 1992; Flamm *et al.*, 2011; Zarrin-Ghalami and Fatemi, 2013; Masquelier, 2014; Duan *et al.*, 2016) and the strain energy W (Beatty, 1964). In a log-log scale, the number of cycles at end-of-life generally decreases linearly when the predictor value increases. Most of the time, tests are performed under relaxing tension loadings. When the mean value of the loading has a significant influence on the results, the Haigh diagram is preferred to the S-N curves. This diagram has widely been used to represent the endurance limit of metals in a $(\sigma_{mean}, \sigma_{amp})$ plot. Considering fatigue of NR at a fixed stress amplitude σ_{amp} , an increase of the mean stress σ_{mean} decreases its lifetime for the $R < 0$ condition, whereas it

increases (*i.e.* it is reinforced) for the $R > 0$ condition. The Haigh diagram is therefore well suitable to gather fatigue data and was first introduced by André *et al.* (1999) to study NR fatigue. Iso-lifetime curves obtained highlighted the influence of σ_{mean} on the rubber fatigue life in a $(\sigma_{mean}, \sigma_{amp})$ plot. The Haigh diagram was then systematically used for characterizing the fatigue reinforcement of crystallizable rubbers (Saintier, 2000; Le Cam, 2005; Bennani, 2006; Oshima *et al.*, 2007; Le Chenadec, 2008; Poisson, 2012; Shangguan *et al.*, 2017). Note that the effect of σ_{mean} can however be represented with Wöhler curves. For example, Bathias *et al.* (1998) represented the mean stress as a function of the fatigue life for different temperatures and Abraham *et al.* (2005) the maximal stress as a function of the fatigue life for different stress amplitudes. For multiaxial fatigue, other predictive approach have been introduced since the 2000's. They are based either on the critical plane approach or on the configurational force. The reader can refer to the comparative study by Andriyana *et al.* (2010) for further information. It should be noted that in the case where tests are performed at temperature, the material behavior may strongly evolve and affect the loading condition applied initially. It is therefore necessary to use a quantity that accounts for such effect. This is precisely discussed in Section 4.

2.2 Results obtained

2.2.1 Effect of the loading conditions and fatigue life reinforcement

As soon as 1940, Cadwell *et al.* (1940) showed the influence of the mean strain on the fatigue life of NR. Indeed, a strong fatigue life reinforcement was observed for loading ratios superior to zero. This reinforcement was corroborated in (Fielding, 1943; Beatty, 1964; André *et al.*, 1999; Saintier, 2000). It was not observed for non-crystallizable rubbers (Fielding, 1943; Beatty, 1964; Lindley, 1974), which suggested that SIC is responsible for this lifetime reinforcement. Figure 1 represents the Haigh diagram built from Cadwell and co-workers data. The lifetime reinforcement occurs for the $R_\epsilon > 0$ condition, the slope of the iso-lifetime curves is positive. For high ϵ_{mean} , damage effect becomes preponderant on the reinforcement due to SIC and the slope of the iso-lifetime curves starts to decrease and becomes negative.

2.2.2 Effect of the temperature

Under quasi-static loadings, the effect of temperature on the mechanical behavior of rubber is twofold:

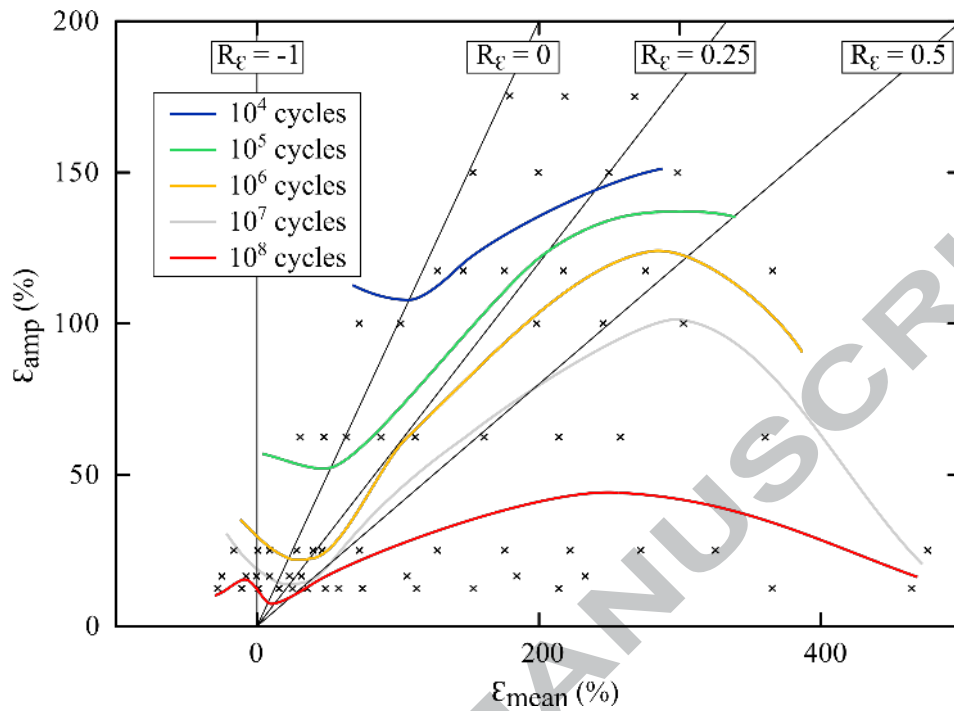


Figure 1. Haigh diagram highlighting the lifetime reinforcement of NR for $R > 0$ for tests performed on cylindrical samples, from data in (Cadwell *et al.*, 1940)

- it modifies its apparent elastic response due to entropic effects and to viscosity. These phenomena act in opposite ways.
- it decreases and limits the crystallinity. Even though Lindley (1974) suggested that NR would behave as a non-crystallizable rubber for a sufficiently high temperature, this result cannot be directly transposable to fatigue because mechanical cycles and more particularly the loading rate can strongly influence SIC. Nevertheless, Treloar (1975) estimated the temperature at which all the crystallites melt between 75 and 115°C. Later, authors showed that SIC almost completely disappeared (*i.e.* crystallinity measured close to zero) for experiments carried out at 75°C (Bruening *et al.*, 2015), 80°C (Albouy *et al.*, 2005; Candau *et al.*, 2015) or 100°C (Trabelsi, 2002), even for large strains. It should be noted that the crystallite melting temperature depends on the stretch: the higher the stretch, the higher the test temperature necessary to melt crystallites (Trabelsi *et al.*, 2002).

Under fatigue loadings, several studies investigated the effect of temperature. For tests carried out at $R = 0$, authors showed that the fatigue resistance of NR decreases as the temperature increases: Lu (1991) showed that NR fatigue life drops by a decade when the temperature increases from 0 to 100°C; for tests performed at a maximal deformation of 250%, Lake and Lindley (1964) measured a loss of fatigue

properties by a factor 4 for similar temperatures; on AE2 samples, Le Chenadec (2008) noted the existence of a temperature threshold at 70°C, from which the NR fatigue resistance (especially under non-relaxing loadings) is affected; on plane samples, Duan *et al.* (2016) showed that the fatigue resistance of NR was only altered for important maximal strains for test carried out at $R_\epsilon = 0$ and in the range of temperature from 23 to 90°C; on Diabolo samples injected with a NR(90%) - BR(10%) blend, Neuhaus *et al.* (2017) measured a shift of the S-N curves towards the decreasing lifetimes as the temperature was increased, independently of the strain applied, for fatigue tests performed at $R_\epsilon = -1$ and for temperatures from 23 to 100°C. Concerning the effect of temperature on the reinforcement, Bathias *et al.* (1998) showed that a lifetime reinforcement was still present at 80°C but occurred for more important mean stress than at 23°C on Diabolo samples, as illustrated in Figure 2. Le Chenadec (2008) measured a decrease of the lifetime reinforcement as the temperature was increased from 5 to 100°C on AE2 samples. Note that only one level of maximum loading was investigated as a function of R , therefore, the reinforcement was only extrapolated over the amplitude of loading range and not measured experimentally. Even though the author highlighted the strong impact of the temperature on the response of the material at elevated temperature, data were analyzed in terms of strain, which can induce a bias. This remark will be further discuss in the result section. Considering the differences in terms of result presented here, the effect of temperature on NR fatigue behavior, especially the link between temperature and SIC during fatigue, remains misunderstood. It is worth noting that NR is highly subjected to self-heating, a difference up to 50°C between the bulk and the surface of a Diabolo has been measured during fatigue experiments (Lu, 1991; Xie, 1992). For this reason, self-heating has to be taken into account in order to analyse the effect of the temperature on the rubber fatigue behavior. Furthermore, investigations including a large range of loading rates could provide additional information on the effect of the temperature on crystallizable rubber fatigue properties. To conclude, fatigue tests carried out at elevated temperature induce thermal and thermo-oxidative aging, i.e. sulfur bond failure and recombination (increase in the material's stiffness), chain scission (decrease in the material's stiffness) and additional vulcanization (increase in the material's stiffness). Some of these phenomena act in opposite ways, which makes difficult the characterization of the material state and its evolution during fatigue.

2.2.3 Damage mechanism

Since the beginning of the 21th century, damage mechanisms on both crystallizable (Saintier, 2000; Bennani, 2006; Le Cam and Toussaint, 2010; Muñoz-Mejia, 2011; Flamm *et al.*, 2011; Poisson, 2012; Le Cam *et al.*, 2013; Masquelier, 2014) and non-

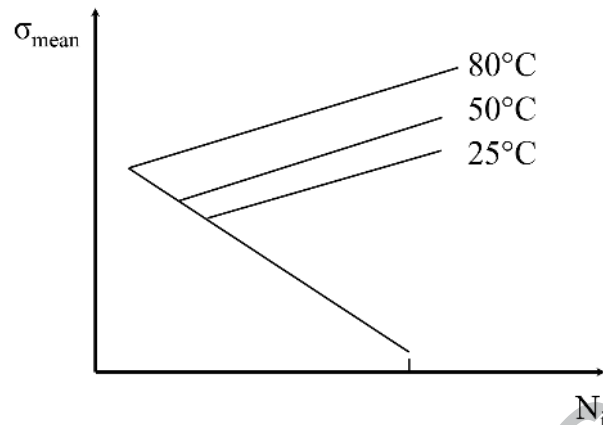


Figure 2. Effect of the temperature on the lifetime reinforcement for tests performed at constant σ_{amp} on Diabolo samples, from Bathias *et al.* (1998)

crystallizable rubbers (Robisson, 2000; Legorju-Jago and Bathias, 2002; Gauchet *et al.*, 2007; Le Cam *et al.*, 2014; Masquelier, 2014) have been investigated by post-mortem Scanning Electron Microscopy (SEM) analyses. For complex loadings performed at 23°C from $R_\epsilon = -0.5$ to 0.5, Le Cam *et al.* (2013) distinguished five macroscopic damage modes under uni- and multi-axial loading conditions and pointed out the strong impact of SIC on the NR fatigue damage resistance. At the microscopic scale, damage occurs in two steps: crack initiation and propagation. For relaxing loadings, the crack initiation at the macroscopic scale is quite similar: the crack initiates in the subsurface in the sample middle section due to a defect that concentrates the stress. The defect can be either a particle part of the rubber formulation (*e.g.* fillers, ZnO), a pollution or a geometrical asperity (*e.g.* joint mold, injection point). The crack propagation, in the case of NR, is signed by SIC markers: wrenchings and striations (Le Cam and Toussaint, 2010; Le Cam *et al.*, 2013). In the case of non-relaxing loading conditions, the striation phenomenon at the fracture surfaces is amplified (see the recent study by Ruellan *et al.* (2018)) and cracks bifurcate at the macroscopic scale. This is summarized in Figure 3: initiation around a defect (A), wrenchings (B), striations (C) and final ligament (D). Neither wrenching nor striation is observed in the case of non-crystallizable rubbers such as SBR (Le Cam *et al.*, 2014). This is the reason why such morphological details are assumed to be due to SIC. Nevertheless, to the best of our knowledge, the damage mechanisms of NR at elevated temperature are not clearly established. Therefore, fatigue tests performed at higher temperatures could provide relevant information on the role of SIC in the fatigue behavior of crystallizable rubbers (Ruellan *et al.*, 2018).

As a conclusion, no study coupled fatigue life measurement at room temperature

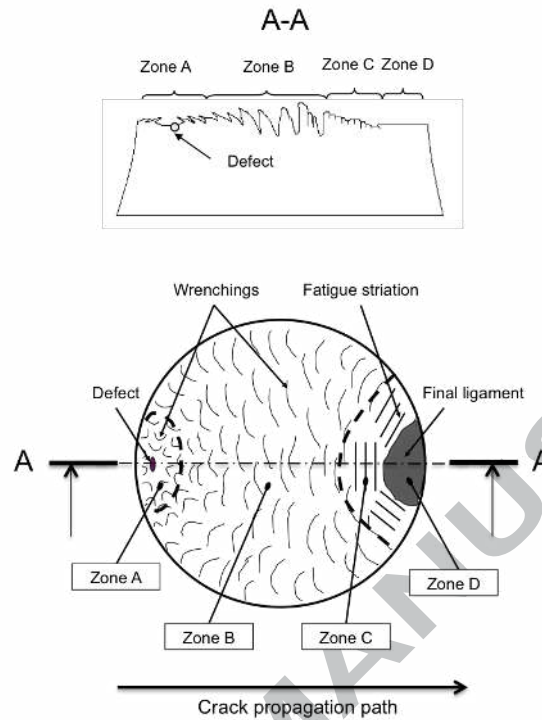


Figure 3. Schematic view of a fracture surface of a filled NR Diabolo sample tested under fatigue loading conditions at $R_e=0$ (a) profile (b) top view (from (Le Cam *et al.*, 2013)) and elevated temperature with an exhaustive damage analysis at both the macroscopic and the microscopic scale for fatigue tests carried out over a large range of loadings, especially non-relaxing ones. This is the motivation of the present study. The next section presents the experimental setup. Then, results are given and discussed. Concluding remarks close the paper.

3 Experimental setup

3.1 Material and sample geometry

The material considered in the present study is a natural rubber (*cis*-1,4 polyisoprene) vulcanised with sulphur and filled with carbon black aggregates. Table 1 summarizes its chemical composition.

Tests were carried out with Diabolo sample. It is presented in Figure 4. As mentioned above, this geometry was firstly introduced by Beatty (1964). Contrarily to

Ingredients	Quantity (phr)
NR	100
Zinc oxide	10
Plastificant	< 3
Carbon black	20-30
Sulphur	1.5
Stearic acid	2
Antioxidant	2-4
Accelerators	2-4

Table 1
Chemical composition of the natural rubber

dumbbell samples, the volume of matter tested is much higher than the critical size of defects leading to crack initiation (typically 200 μm maximum in mean diameter), which reduces the results dispersion and enables the SIC to occur homogeneously. Moreover, in dumbbell sample, the end-of-life criterion is difficult to establish due to the fact that the crack propagation phase is short, therefore it is often chosen as the sample failure. This induces additional dispersion on the fatigue lifetime.

3.2 Loading conditions

The fatigue tests were performed under prescribed displacement with a uni-axial MTS Landmark equipped with a home-made apparatus. The force capacity of the testing machine coupled with the apparatus presented in Figure 4(b), enables us to test eight Diabolo samples simultaneously and independently (*i.e.* with eight force cells), which strongly reduces the fatigue campaign duration.

The relation between the local strain and the macroscopic displacement was calculated by FEA. In order to investigate the influence of the loading on the fatigue life, different loading ratios R_e were applied. They are presented with the corresponding minimum and maximum strains in Table 2. It is recalled that a loading ratio inferior, equal and superior to zero corresponds to tension-compression, repeated tension and tension-tension test, respectively. In practice, fatigue tests are carried out until failure.

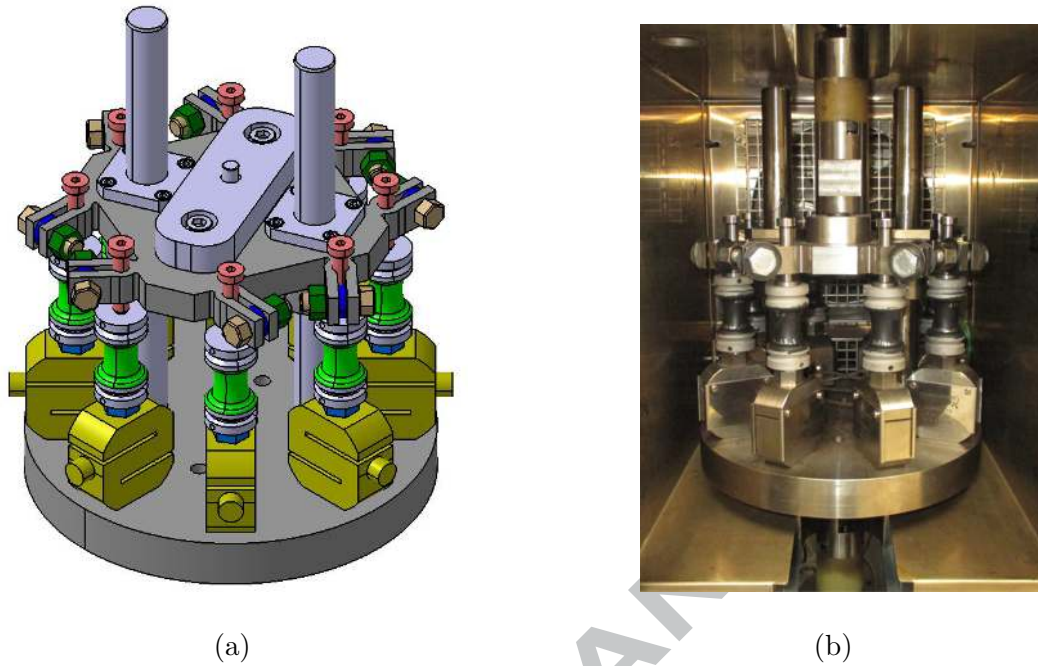


Figure 4. Experimental setup: (a) CAD design; (b) home-made apparatus for testing eight samples simultaneously and independently

The frequency was chosen in such a way that the global strain rate $\dot{\epsilon} = (\epsilon_{max} - \epsilon_{min}) \times f$, *i.e.* whatever the signal shape, was constant and equal to a value between 1.8 s^{-1} and 2.4 s^{-1} , depending on the strain amplitude. This limited the material self-heating so that no thermal damage was superimposed to the mechanical damage. In practice, this led to a maximum temperature variation (self-heating) measured at the sample surface equal to 20°C (in case if tests performed at 23°C). It should be noted that even though the temperature in the bulk is much higher than in surface, convection occurs and limits the temperature raise. This is for instance the case in the crack tip zone, where the mechanisms of crack growth take place.

3.3 Lifetime criterion

The number of cycles at crack initiation, denoted N_i , is based on the maximal reaction force evolution. As illustrated in Figure 5, three regimes were obtained during the fatigue test: a significant decrease in the maximal reaction force due to stress softening, its stabilization and its drop (brutal or not, depending on the loading and environmental conditions). N_i corresponds to the number of cycles at

R_ϵ	ϵ_{min} (%)	ϵ_{max} (%)	Frequency (Hz)
-0.25	-18	72	2.5
	-25	100	1.5
0	0	60	3
	0	90	2.5
	0	120	1.5
	0	150	1.5
0.125	8.75	70	4
	12.5	100	2.5
	17.5	140	2
	21.5	172	1.5
0.25	17.5	70	4
	30	90	3
	40	150	2
	43	172	1.5
	50	200	1.5
	62.5	250	1
0.35	70	200	1.5
	48.5	139	2.5
	65	186	1.75
	70	200	1.5
	81	231	1.5

Table 2
Uni-axial loading conditions

the end of the plateau, when the derivative of the maximal reaction force F_{max} is no longer constant. It is similar to criterion (iv) presented in Section 2.1.3. In practice, it corresponds to the occurrence of a macroscopic crack whose length is inferior to 5 mm at the sample surface. Note that numerous sub-millimetric cracks appeared at the sample surface soon during the test (about half of N_i), without propagating.

3.4 Microscopy

Second electron images of Diabolo fracture surfaces were recorded with a JSM JEOL 7100 F scanning electron microscope (SEM). In addition, the SEM was coupled with an Oxford Instrument X Max Energy Dispersive Spectrometer of X-rays (EDS) and an Azttec software in order to determine the surface fracture composition, especially in the crack initiation zone. The Diabolo fracture surfaces were cut with a razor blade into cylindrical pieces which did not exceed 1 cm in

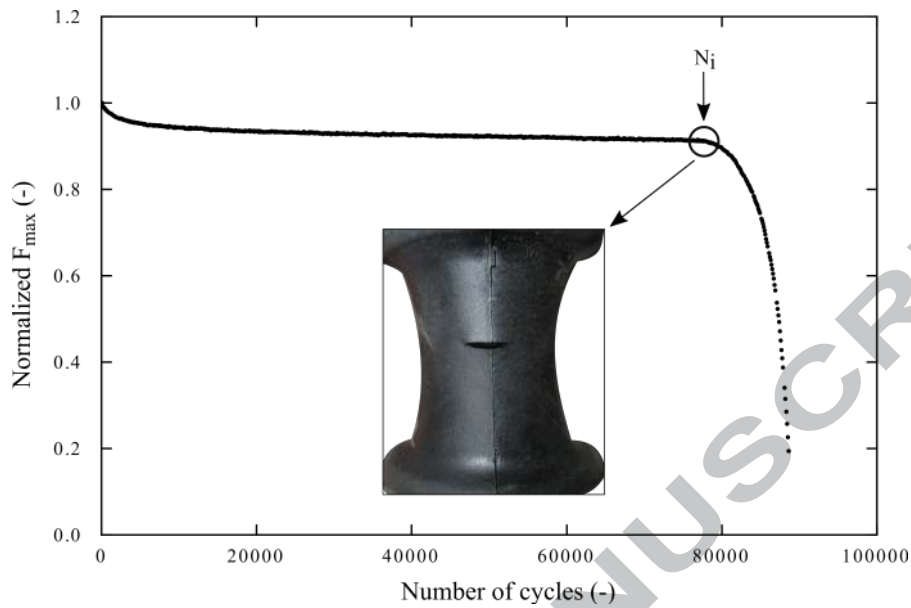


Figure 5. Force evolution versus the number of cycles

height. Since rubber does not conduct electrons enough, fracture surfaces to be analyzed were previously metallized by vapour deposition of an Au-Pd layer.

An optical microscope Keyence VHX 5000 was used and equipped with two lens to cover magnifications from $\times 1$ to $\times 5000$. Unlike SEM, the fracture surfaces did not require any preparation.

4 Results and discussion

Fatigue tests are generally performed at room temperature. Only a few studies investigated the effects of test temperature on uniaxial fatigue response. In these studies, tests were performed under controlled displacement (Cadwell *et al.*, 1940; Fielding, 1943). In Bathias *et al.* (1998), results are presented in terms of stress, but no information is provided neither on its calculation nor on the prescribed signal. At this stage, a discussion on the relevant quantity to use for processing fatigue data is required. Filled rubber materials exhibit viscoelasticity, so that for a given displacement, the force obtained at different temperatures changes. This questions the choice between the displacement (or the strain) or the force (or the stress) to process fatigue data. Typically for fatigue tests prescribed under displacement, as the material stiffness decreases when temperature is increased, the fatigue damage can be significantly different from tests performed under pre-

scribed force. This question has not been addressed in the literature, since tests are generally performed at room temperature. This is all the more important when considering non-relaxing loadings. This is illustrated in Figure 6.

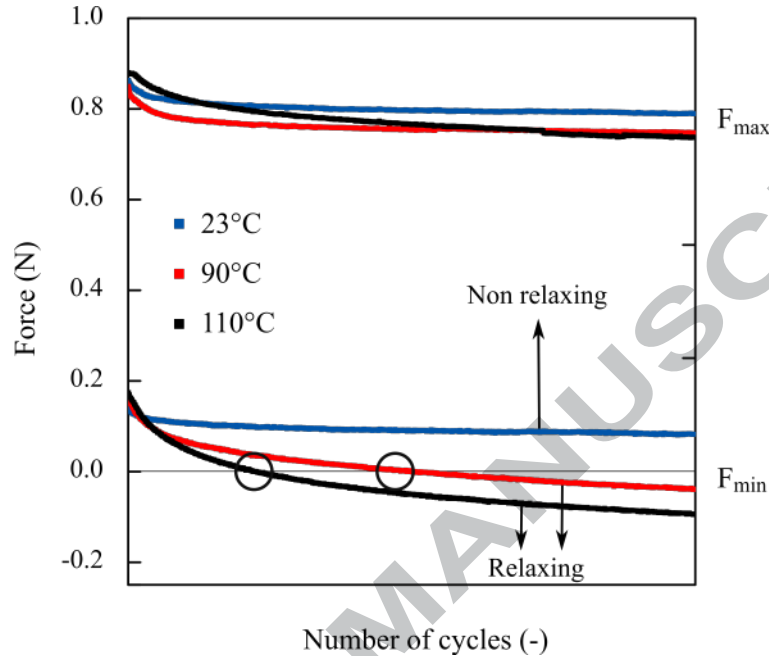


Figure 6. Evolution of the maximum and minimum values of the force for non-relaxing loading conditions prescribed under displacement

This figure shows the evolution of the maximum and minimum force during an *a priori* non-relaxing fatigue test carried out at $R_\epsilon = 0.125$ prescribed under displacement for different temperatures, namely 23, 90 and 110°C. At 23°C (in blue on Fig. 6), the minimum force stabilizes at a value higher than 0 N. Therefore, the loading remains non-relaxing, whatever the quantity used (displacement or force). However, if the temperature is increased, the loading becomes relaxing (*i.e.* the minimum force is lower than 0 N), which affects the lifetime reinforcement. The transition from a positive to a negative value of F_{min} , *i.e.* from a non-relaxing to a relaxing loading condition, is shown by the black circles in Fig. 6. The force is therefore the most appropriate quantity to analyze the reinforcement due to SIC at elevated temperatures.

Remark #1: of course, designing rubber parts requires the use of predictive approach involving the stress (Andriyana et al., 2010). In the present case, the model used to calculate the stress with finite element code should account for time-dependency, stress softening, permanent set, stress-induced crystallization and the effects of temperature on these phenomena. This is not the goal of the present study.

In the following, fatigue behavior of NR is first described for tests performed at 23°C before being compared with fatigue behavior obtained at higher temperatures (namely 90 and 110°C). Results are presented in terms of both lifetime and damage mechanism.

4.1 Reference tests performed at 23°C

4.1.1 Fatigue lifetime

First of all, Figure 7 illustrates the dispersion obtained for the number of cycles at crack initiation, here for tests carried out at $R_\epsilon = 0$ and $T = 23^\circ\text{C}$. The circles represent the individual tests, the black squares correspond to their mean values. In the following, only the mean lifetimes and the mean forces will be considered. Iso-lifetime curves are plotted in the Haigh diagram in Figure 8. It should be noted that a filled square corresponds to the average value of eight fatigue tests. The iso-lifetime curves are given in relation to the amplitude and the mean value of the loading, and are determined by interpolation from the different points (filled squares), which explains why they do not systematically pass through the filled squares. The iso-line curves are denoted N_1 to N_4 . They correspond to lifetime ranging between 10^4 and 10^6 cycles, with $N_1 < N_2 < N_3 < N_4$. Each square in the diagram represents a mean fatigue life between eight tests.

Four zones can be distinguished:

- $-0.25 < R_F < 0$ (tension-compression). The iso-lifetime curves are decreasing monotonously and are perpendicular to the $R_F = 0$ line, suggesting that F_{max} is the parameter driving the damage. This is in good agreement with results obtained by Cadwell *et al.* (1940).
- $0 < R_F < 0.125$ (tension-tension). The slope of the iso-lifetime curves increases in absolute value.
- $0.125 < R_F < 0.25$. The slope of the iso-lifetime curves becomes positive, which corresponds to a strong lifetime reinforcement: at a given F_{amp} , the lifetime increases when F_{mean} is increased, *i.e.* when F_{max} increases.
- $R_F > 0.25$. Iso-lifetime curves are parallel, their slopes are positive and roughly equals.
- Red crosses stand for experiments stopped after at least 10^6 cycles, when no macroscopic crack was self-initiated. This zone where the number of cycles at crack initiation is superior to 10^6 highlights how beneficial is the increase of the minimum force as the maximum force also increases.

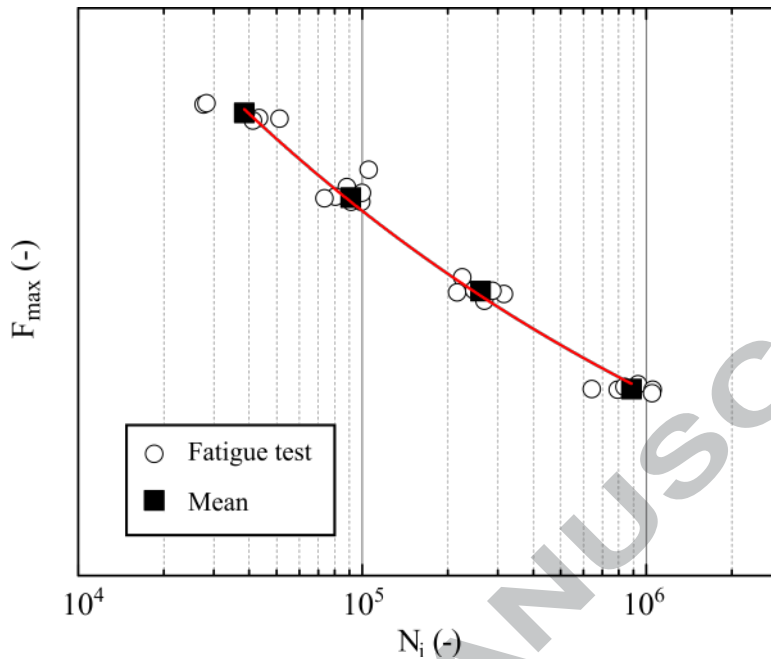


Figure 7. Endurance curve for tests carried out at $R_e = 0$ and $T = 23^\circ\text{C}$

At a given F_{max} , an increase of F_{min} goes along with a reinforcement amplification. Non-relaxing loadings are therefore a SIC-induced reinforcement promoter (Beurrot-Borgarino *et al.*, 2013). For relaxing loadings ($R_F < 0$), results suggest that crystallites that could have formed during loading melt during the unloading and the reinforcement effect due to SIC is cancelled at each cycle. This is consistent with results obtained for non-crystallizable rubbers such as styrene butadiene rubbers (SBR), for which increasing the mean force leads to decrease the life time whatever the loading ratio considered. Moreover, it should be noted that in the studies investigating fatigue with XRD, the loading ratio at which the fatigue life reinforcement occurs is not provided (Bruening *et al.* (2012), Beurrot-Borgarino *et al.* (2013), Candau *et al.* (2015)). Nevertheless, as reported by Saintier *et al.* (2011) for non-relaxing loading, a "cumulative process" takes place and it is believed that the crystallinity level remains superior to zero at any time during a non-relaxing loading, which could explain the lifetime reinforcement (see Fig. 11(b) in Saintier *et al.* (2011)). Therefore, it would have been relevant to link the value of the loading ratio from which the reinforcement is observed to the crystallinity variation during the mechanical cycle by using XRD, but the diabolo shaped specimen makes it difficult.

Figure 9 shows that the heat built-up is limited, since the self-heating measured at the surface of the sample does not exceed 20°C . What is quite remarkable is the fact that non-relaxing conditions have no real effect on the self-heating. This

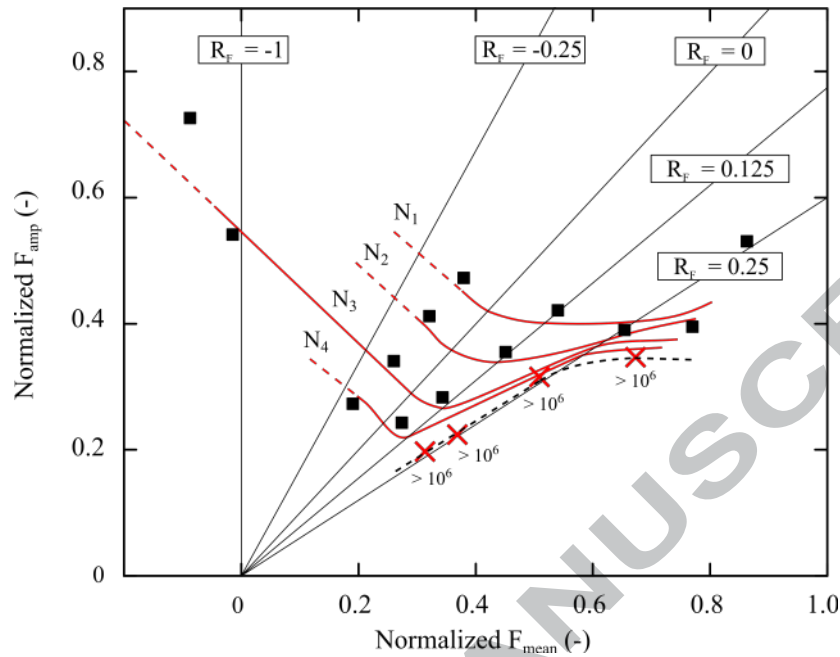


Figure 8. Haigh diagram at 23°C

is highlighted by the horizontal dotted line. Along this line, the loading amplitude is constant, the frequency applied is the same and approximately the same temperature increases are obtained. The only difference is the value of the mean loading. When increasing, it promotes SIC-induced reinforcement. The fact that the self-heating is not affected by SIC effects is logical because crystallization/melting process does not produce heat over one mechanical cycle (see Samaca Martinez *et al.* (2013) and Le Cam (2017)). This shows that linking self-heating to end-of-life in case of crystallizable rubbers is delicate.

4.1.2 Post-mortem analysis

Post-mortem analyses provide important information on damage mechanisms leading to the sample failure. In this section, macroscopic damage is first investigated by linking loading and damage at the macroscopic scale in the Haigh diagram. Then, the damage is studied at the microscopic scale.

4.1.2.1 Macroscopic scale

Post-mortem analyzes of the failed samples have been carried out. Three fatigue damage modes have been identified. They are presented in Figure 10. Damage at

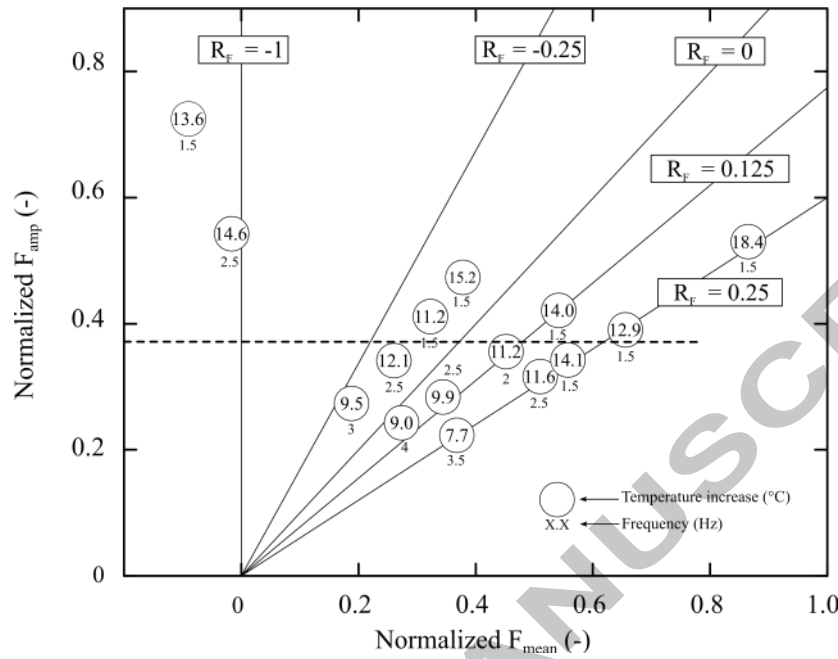


Figure 9. Self heating cartography in the Haigh diagram for tests carried out at 23°C the macroscopic scale is described as follow:

- **Damage mode 1:** the failure occurred perpendicularly to the stretching direction, in the section of minimum radius (the middle of the sample). It was observed for $R_F \leq 0.125$.
- **Damage mode 2:** the macroscopic crack propagated in the medium region. Contrary to Damage mode 1, numerous cracks initiated (see the red dots) without propagating. Eventually, a crack predominated and propagated. The crack propagation is characterized by a bifurcation phenomenon that could be compared to what was previously observed and called branching in Le Cam *et al.* (2013) (fatigue damage mode 6 and 7) and seems to indicate that the reinforcement due to SIC is activated.
- **Damage mode 3:** it corresponds to a cohesive failure under the insert. This damage mode was observed on Diabolo samples tested at $R_\varepsilon \geq 0.25$ and at important loading amplitudes. The fact that no failure occurred in the medium section suggests that the reinforcement due to SIC was very important in this zone, therefore the crack initiation zone was shifted under the metallic insert where the hydrostatic pressure is high.

4.1.2.2 Microscopic scale

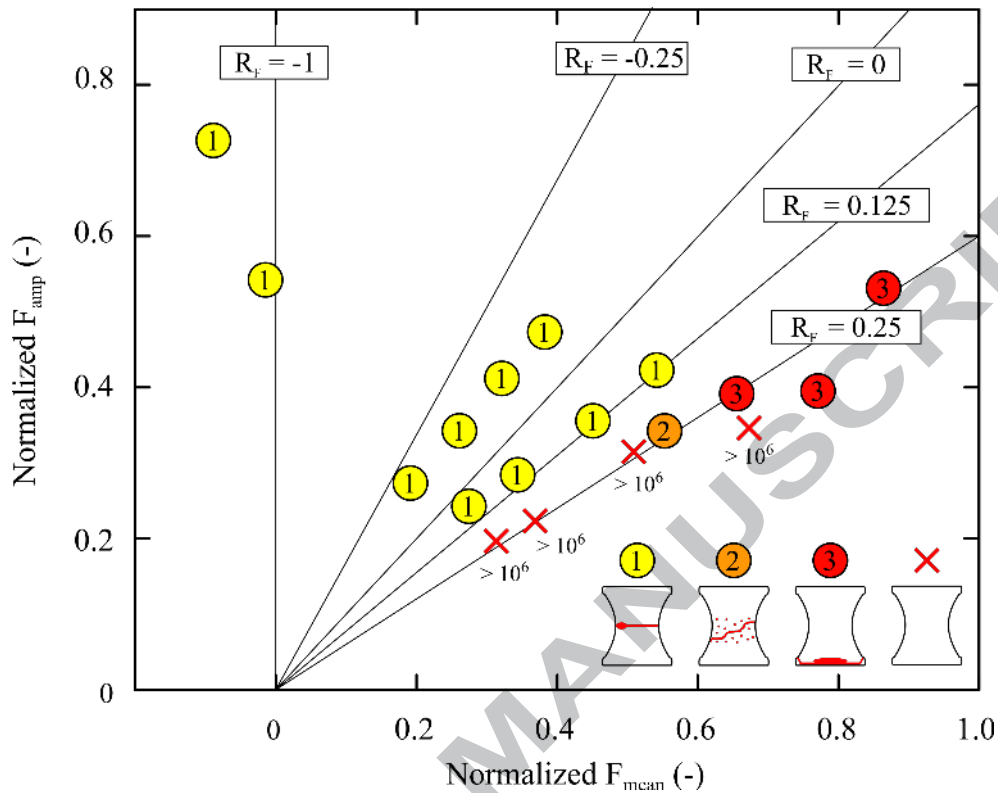


Figure 10. Cartography in a Haigh-like diagram of the macroscopic damage obtained for fatigue tests at 23°C

Damage mode presented in section 4.1.2.1 are more precisely investigated at the microscopic scale:

- Damage mode 1:** in most cases, the crack initiated around a carbon black agglomerate whose radius does not exceed 200 μm (see Figure 11(a)). The crack propagated around the defect by forming an elliptical zone, it reached the sample surface and propagated into the bulk. The propagation zone exhibits wrenchings whose size increased throughout the propagation. As defined by Le Cam *et al.* (2004), wrenchings are triangular-shaped areas. They form from highly stretched ligaments at the crack tip that break and shrink. When the stress level increased at the crack tip, wrenchings gave way to striations in a continuous process (see Fig. 11(b)). As neither wrenchings nor striations were observed in non crystallizable rubbers, they were assumed to be due to SIC (Le Cam and Toussaint, 2010). Two regimes of striations form throughout the propagation. This is more precisely detailed and discussed in Ruellan *et al.* (2018). Finally, when the stress exceeds the stress at break, the final ligament failed. Its very smooth surface is similar to fracture surfaces obtained under

quasi-static loading condition. Figure 12 illustrates fatigue damage mode 1. It is consistent with previous observation in the literature (Saintier, 2000; Bennani, 2006; Le Cam *et al.*, 2008; Le Cam and Toussaint, 2010; Masquelier, 2014).

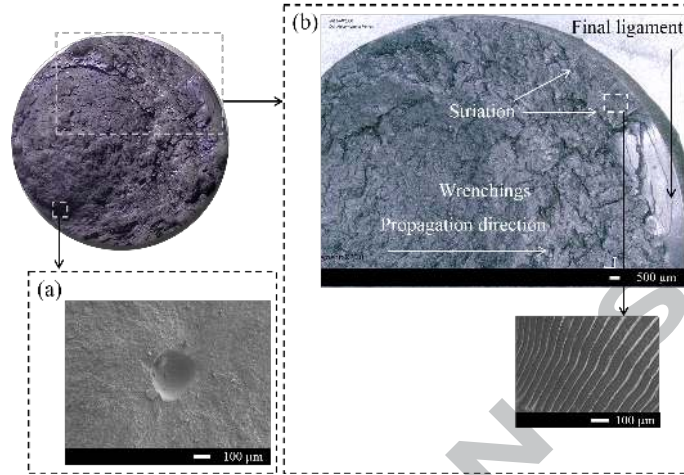


Figure 11. Damage mode 1 microscopic illustration at 23°C: (a) crack initiation; (b) crack propagation

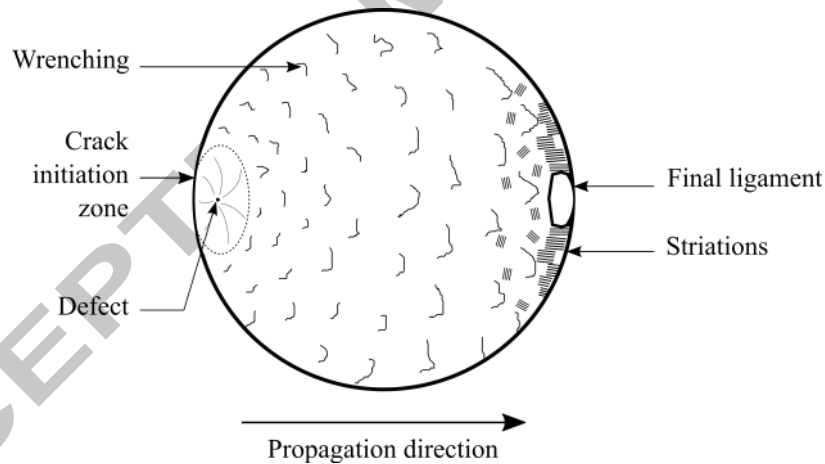


Figure 12. Schematic view of the fracture surface at 23°C

- **Damage mode 2:** the multi-crack initiation observed on the Diabolo surface at the macroscopic scale also manifested at the microscopic scale. Indeed, Figure 13(a) shows the presence of numerous patterns referred to as "cones" in the following. They were observed all over the sample fracture surface without preferred localisation, suggesting that cones formed before a macroscopic crack propagated. Cones are oriented parallelly to the stretching direction. Eventually, a crack propagated into the bulk as testify the wrenchings in between them.

Figure 13(b) focuses on a cone. One can remark a flat surface on the top of it corresponding to the initiation zone. The cone shape is provided by the fact that, because of the high local crystallinity kept throughout the fatigue cycle, the crack could not propagate into the bulk (*i.e.* perpendicular to the stretching direction). Hence, it grew toward the direction of least energy, almost parallelly to the stretching direction. The presence of striations confirms the high level of crystallinity around cones. This type of fatigue damage has never been observed previously.

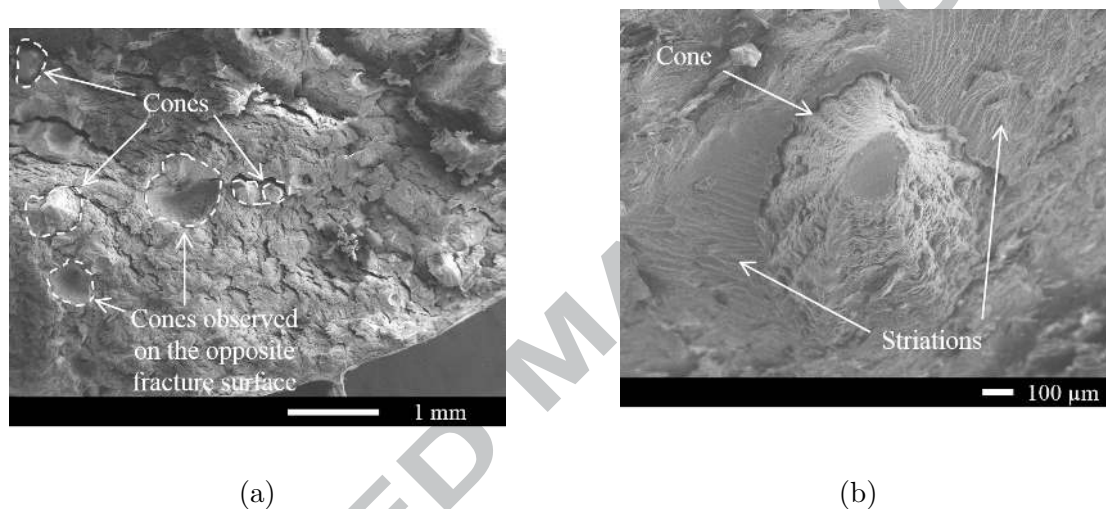


Figure 13. Damage mode 2 microscopic illustrations: (a) initiation of secondary cracks; (b) zoom on a cone

- **Damage mode 3:** The cohesive failure in the rubber matrix located below the metallic insert was due to multi-cavitation that weakened the interface, at the microscopic scale, as shown in Figure 14. These cavitation zones are similar to those observed by Le Cam *et al.* (2008, 2013) for comparable loading conditions. Note that no striation was observed.

As a summary, at $T = 23^{\circ}\text{C}$, a lifetime reinforcement was observed for non-relaxing loading conditions. By the mean of both macroscopic and microscopic fracture surface analysis, SIC is found to contribute mostly to this phenomenon. The formation of striations and cones is likely driven by SIC. As crystallinity decreases with temperature (Trabelsi *et al.*, 2002), the question now is to define how the fatigue life reinforcement due to SIC is impacted by an increase in the material's temperature.

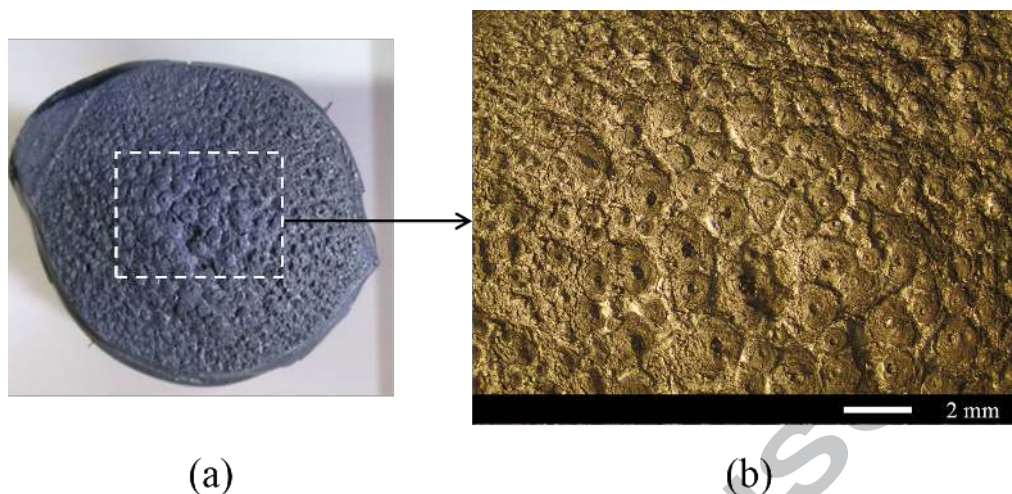


Figure 14. Damage mode 3 microscopic illustrations: (a) multi-cavitation under the inserts; (b) zoom on cavitations

4.2 Fatigue tests performed at 90°C

Fatigue tests were carried out at 90°C and the fracture surfaces were analysed at both the macroscopic and microscopic scale. The effect of the temperature on the rubber fatigue properties is presented in the following sections.

4.2.1 Lifetime

Results are presented in Figure 15 and can be summed up as follow:

- $-0.25 < R_F < 0$ (tension-compression). Similarly to tests performed at 23°C, the iso-lifetime curves are decreasing, meaning that F_{max} drives the fatigue damage. Nevertheless, the fatigue lifetime drops by a factor 2 at $R_F = 0$ when the temperature increases from 23 to 90°C (the slope of the curve is higher in absolute value). This result is in good agreement with the literature (Lake and Lindley, 1964; Neuhaus *et al.*, 2017).
- $0 < R_F < 0.25$ (tension-tension). A lifetime reinforcement is observed, it is more significant for the highest lifetimes. For a given value of F_{mean} , the reinforcement at 90°C is not as important as at 23°C. These results seem to indicate that SIC still plays a role in the fatigue behavior at 90°C, while crystallites are generally assumed to be melted at this temperature in case of quasi-static loading (Candau *et al.*, 2015).
- $0.125 < R_F < 0.25$. The reinforcement is less pronounced.

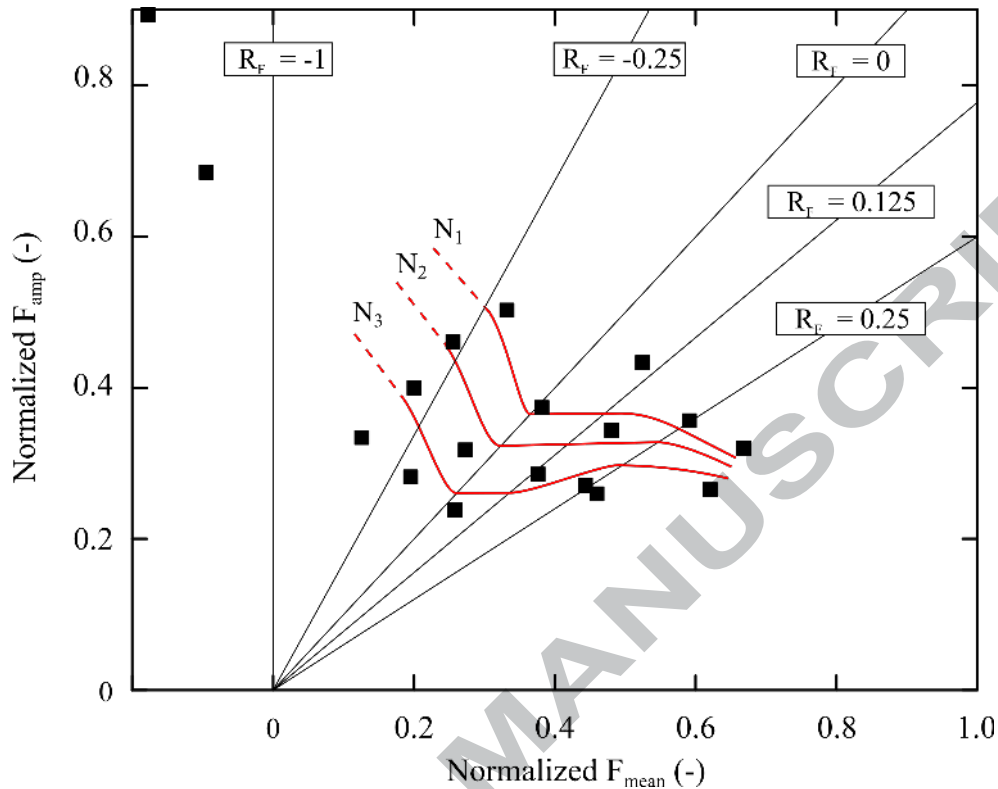


Figure 15. Haigh diagram at 90°C

Concerning the number of cycles of crack propagation, it was inferior to 100 cycles whatever the loading applied. This clearly shows SIC delays crack initiation, even for low values of crystallinity, but does not resist the crack propagation at the macroscopic scale anymore.

It should be noted that due to technical considerations, no self-heating measurement was performed at elevated temperatures.

4.2.2 Post-mortem analysis

A unique macroscopic damage mode was observed at 90°C. It is similar to Damage mode 1 at 23°C, described in section 4.1.2. One recalls that Damage mode 1 corresponds to a crack perpendicular to the stretching direction, in the section of minimum radius.

At the microscopic level, the crack initiation is similar to 23°C, but the propagation differs. The damage mechanisms at 90°C are illustrated in Figure 16 and can be described as follows:

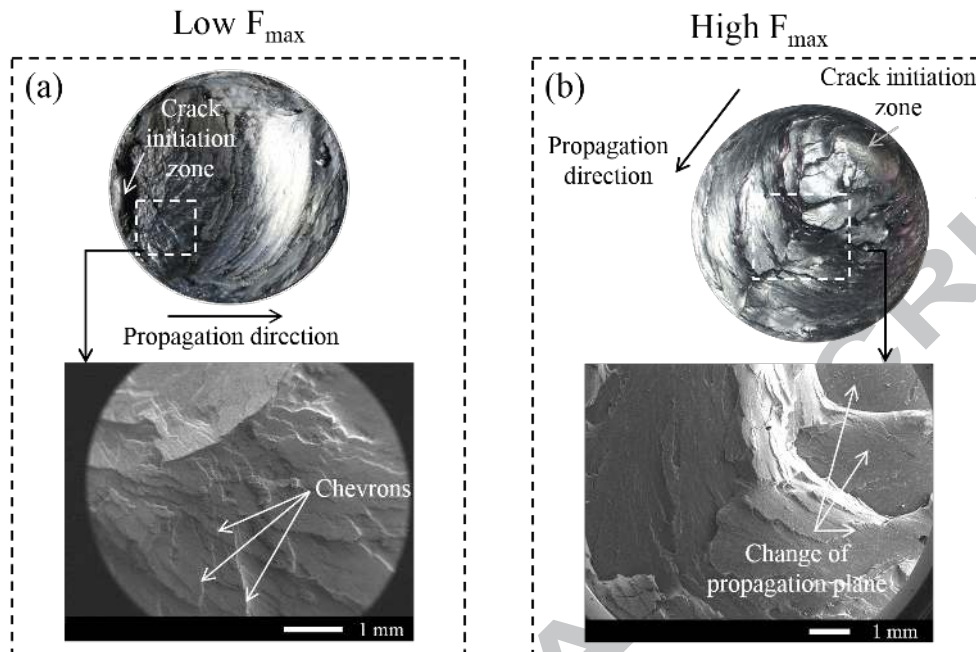


Figure 16. Crack propagation at 90°C: (a) chevrons at low F_{max} ; (b) changes in the propagation plane at high F_{max}

- a crack initiates around a defect and propagates elliptically up to the surface, similarly to 23°C,
- after reaching the surface, the crack propagates through the bulk. From this stage, two propagation modes are identified: (i) for low values of F_{max} , the crack propagates in the same plane, which is perpendicular to the loading direction. "Chevrons" patterns are observed, in the early propagation phase (see Fig. 16(a)). Chevrons are V-shaped areas that classically form in non-crystallized rubbers (This pattern has already been reported in the literature on SBR (Le Cam, 2005), which is non-crystallizable). The rest of the sample is rather flat; (ii) for high values of F_{max} , no chevron forms. Crack propagates with significant changes in the propagation plane. Each propagation plane remains perpendicular to the loading direction (see Fig. 16(b)). The brutal drop in force during the fatigue test confirms that at this test temperature the crack propagation rate is high.

The crack initiation (localisation, defect type) is not affected by the increase of the test temperature. However, the crack propagation is strongly influenced by the crystallinity decrease that may be related to the disappearance of SIC markers, in comparison to tests performed at 23°C.

Although a lifetime reinforcement still occurs at 90°C, no SIC marker is observed.

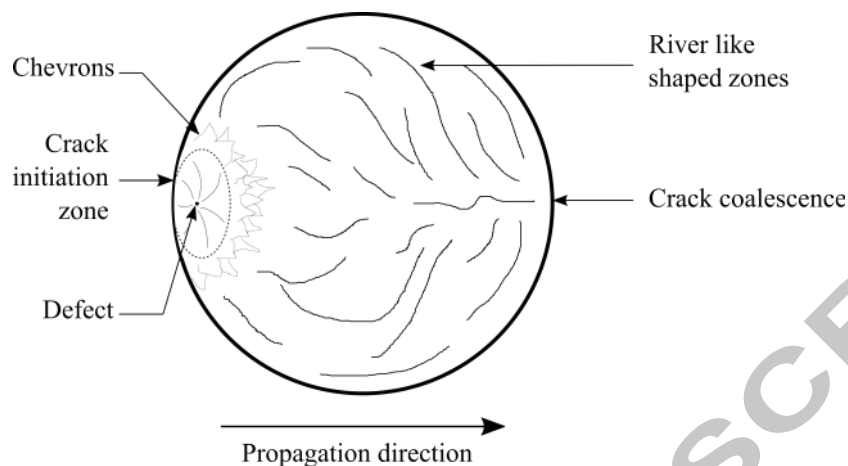


Figure 17. Damage description at 90°C. Chevrons and rivers replace wrenchings and striations

This observation highlights that SIC could induce a reinforcement even for low crystallinity values. Nevertheless, low crystallinity level is not sufficient to enable SIC markers to form.

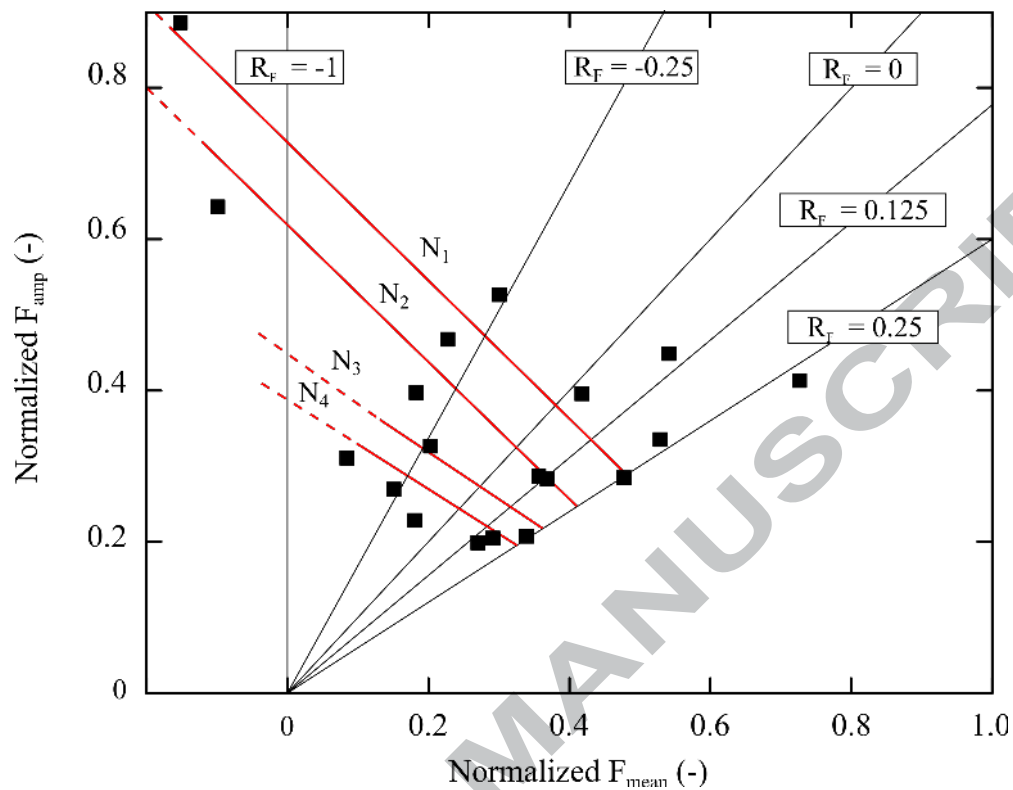
4.3 Fatigue tests performed at 110°C

Results obtained are presented in the Haigh diagram in Figure 18. The iso-lifetime curves decrease monotonously, meaning that F_{max} drives the rubber fatigue life. The damage mechanisms are similar to the one described for tests carried out at 90°C. Therefore, considering both fatigue lives and damage mechanisms, it seems that SIC has totally disappeared at 110°C, as it does not delay crack initiation anymore.

4.4 Conclusion

Figure 19 presents a Haigh diagram where the iso-lifetime curves of tests carried out at 23, 90 and 110°C are reported in red, blue and green, respectively. For the sake of clarity, only two isolines are plotted. Several points can be mentioned and discussed:

- SIC plays a role of paramount importance in NR fatigue resistance. At 23°C, an important lifetime reinforcement was observed for non-relaxing loading conditions and attributed to SIC. This result was corroborated by the presence of



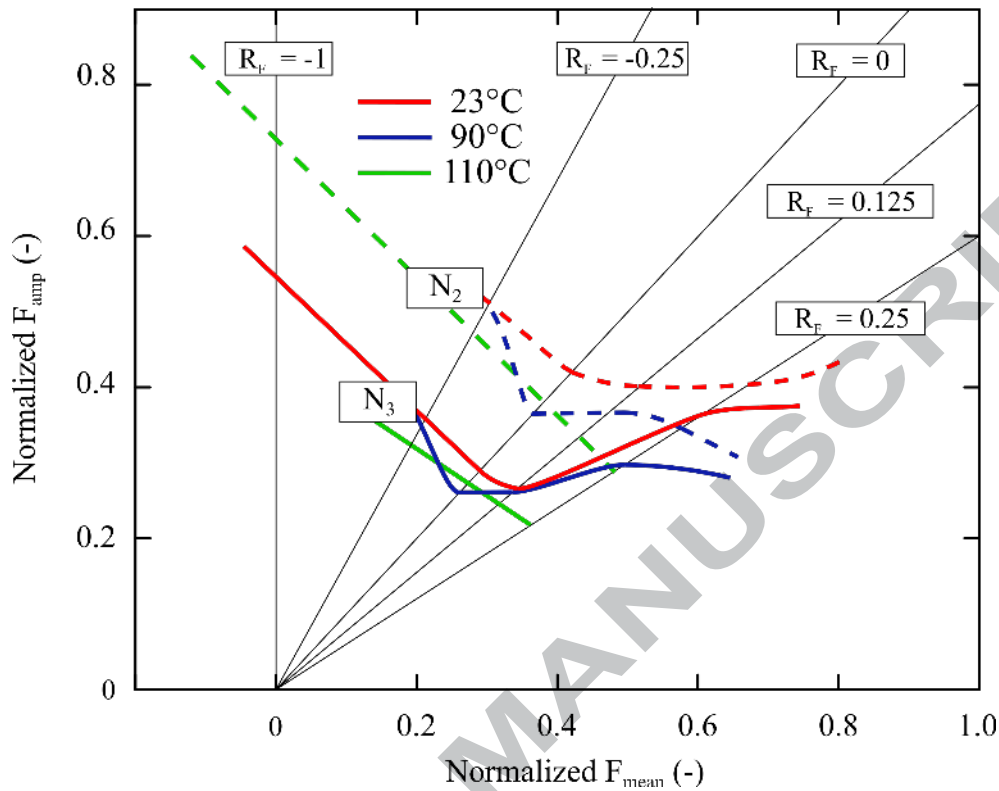


Figure 19. Haigh diagram at 23, 90 and 110°C in red, blue and green, respectively

5 Conclusion

The present study investigates temperature effects on the fatigue life reinforcement due to SIC for non-relaxing loadings. In the first part of the paper, a brief state of the art points out the lack of experimental results in this field and the necessity to carry out additional fatigue tests, especially under non-relaxing loading conditions and elevated temperatures. A wide range of uni-axial fatigue tests including loading ratios from -0.25 to 0.35 were performed with a filled NR at 23, 90 and 110°C using a multi-post home-made apparatus. Both lifetimes and damage mechanisms were considered and mapped in Haigh diagrams. As expected, a strong lifetime reinforcement was obtained for the reference tests carried out at 23°C. Fatigue damage was described at the macroscopic scale and mapped in the Haigh diagram. Fatigue damage mechanisms were then investigated at the microscopic scale, where the signature of reinforcement due to SIC on the fracture surfaces has been identified. Typically, fatigue striations and cones peopled the fracture surfaces obtained under non-relaxing loading conditions. At 90°C, fatigue life reinforcement was still observed. It is lower than at 23°C. Nevertheless, only

one damage mode was observed at the macroscopic scale. At the microscopic scale, fracture surfaces looked like the ones of non-crystallizable rubbers. At 110°C, the fatigue life reinforcement totally disappeared. It is believed that this is due to the disappearance of SIC at such temperature level. It should be noted that aging also reduces the ability of material to crystallize under tension (see Grasland *et al.* (2017)) and further investigations have to be carried out to characterize the effect of the loading rate on aging.

To conclude, questions of importance remain unanswered on the role of SIC in the lifetime reinforcement process: *(i)* what is the precise conditions for fatigue-induced SIC promotion? *(ii)* What is the minimum crystallinity level required to ensure a reinforcement? *(iii)* what is the effect of multi-axial loadings on the reinforcement due to SIC at elevated temperature? *(iv)* how SIC reinforcement is altered by aging during fatigue at elevated temperature? These questions are currently addressed in our lab.

6 Acknowledgements

The authors thank the Cooper Standard France company for supporting this work and for fruitful discussions. The authors thank also the National Center for Scientific Research (MRCT-CNRS and MI-CNRS) and Rennes Metropole for supporting this work financially. SEM images were performed at CMEBA facility (ScanMAT, University of Rennes 1) which received a financial support from the European Union (CPER-FEDER 2007-2014).

References

- Abraham, F., Alshuth, T., and Jerrams, S. (2005). The effect of minimum stress and stress amplitude on the fatigue life of non-strain crystallising elastomers. *Materials and Design*, **26**, 239–245.
- Albouy, P. A., Marchal, J., and Rault, J. (2005). Chain orientation in natural rubber, part i: The inverse yielding effect. *The European Physical Journal E*, **17**, 247–259.
- André, N., Cailletaud, G., and Piques, R. (1999). Haigh diagram for fatigue crack initiation prediction of natural rubber components. *KGK-Kautschuk Gummi Kunststoffe*, **52**, 120–123.
- Andriyana, A., Saintier, N., and Verron, E. (2010). Configurational mechanics and

- critical plane approach: Concept and application to fatigue failure analysis of rubberlike materials. *International Journal of Fatigue*, **32**, 1627 – 1638.
- Ayoub, G. (2010). *Comportement en grandes déformations et fatigue des polymères : modélisation constitutive et prédiction de la durée de vie en fatigue*. Ph.d thesis.
- Bathias, C., Le Gorju, K., Lu, C., and Menabeuf, L. (1997). Fatigue crack growth damage in elastomeric materials. In R. S. Piascik, J. C. Newman, and N. E. Dowling, editors, *Fatigue and fracture*, volume 27, pages 505–513. ASTM STP1296.
- Bathias, C., Houel, P., N'Faly Berete, Y., and Le Gorju, K. (1998). Damage characterization of elastomeric composites using X-ray attenuation. In K. L. Reifsnider, D. A. Dillard, and A. H. Cardon, editors, *Fatigue and fracture*, volume Progress in durability analysis of composite systems: Third International Conference, 1997, pages 103–110. Balkema.
- Beatty, J. R. (1964). Fatigue of rubber. *Rubber Chemistry and Technology*, **37**, 1341–1364.
- Bennani, A. (2006). *Elaboration, comportement et durée de vie en fatigue du caoutchouc naturel renforcé de silice*. Ph.d. thesis, Ecole Nationale Supérieure des Mines de Paris.
- Beurrot-Borgarino, S., Huneau, B., Verron, E., and Rublon, P. (2013). Strain-induced crystallization of carbon black-filled natural rubber during fatigue measured by in situ synchrotron x-ray diffraction. *International Journal of Fatigue*, **47**, 1–7.
- Bruening, K., Schneider, K., Roth, S. V., and Heinrich, G. (2015). Kinetics of strain-induced crystallization in natural rubber: A diffusion-controlled rate law. *Polymer*, **72**, 52 – 58.
- Cadwell, S. M., Merrill, R. A., Sloman, C. M., and Yost, F. L. (1940). Dynamic fatigue life of rubber. *Industrial and Engineering Chemistry (reprinted in Rubber Chem. and Tech. 1940;13:304-315)*, **12**, 19–23.
- Candau, N., Laghmach, R., Chazeau, L., Chenal, J.-M., Gauthier, C., Biben, T., and Munch, E. (2015). Temperature dependence of strain-induced crystallization in natural rubber: On the presence of different crystallite populations. *Polymer*, **60**, 115 – 124.
- Duan, X., Shangguan, W.-B., Li, M., and Rakheja, S. (2016). Measurement and modelling of the fatigue life of rubber mounts for an automotive powertrain at high temperatures. *Proceedings of the Institution of Mechanical Engineers, Part D: Journal of Automobile Engineering*, **230**, 942:954.
- Fielding, J. H. (1943). Flex life and crystallisation of synthetic rubber. *Industrial and Engineering Chemistry*, **35**, 1259–1261.
- Flamm, M., Spreckels, J., Steinweger, T., and Weltin, U. (2011). Effects of very high loads on fatigue life of nr elastomer materials. *International Journal of Fatigue*, **33**, 1189 – 1198.

- Gauchet, S., Le Gorju, K., and Ranganathan, N. (2007). Influence du noir de carbone sur les mécanismes de rupture par fatigue de caoutchouc hnbr. *18ème Congrès Français de Mécanique (Grenoble 2007)*.
- Grasland, F., Chenal, J., Chazeau, L., Caillard, J., and Schach, R. (2017). Role of strain-induced crystallization on fatigue properties of natural rubber after realistic aerobic ageing.
- Greensmith, H. W. (1956). Rupture of rubber - iv - tear properties of vulcanized containig carbon black. *Journal of Polymer Science*, **21**, 175–187.
- Greensmith, H. W. and Thomas, A. G. (1956). Rupture of rubber - iii - determination of tear properties. *Rubber Chemistry and Technology*, **29**, 372–381.
- Kim, H. J., Song, M. W., Moon, H. I., Kim, H., and Kim, H. Y. (2004). Fatigue life prediction of a rubber material based on dynamic crack growth considering shear effect. *International Journal of Automotive Technology*, **15**, 317–324.
- Lake, G. J. (1995). Fatigue and fracture of elastomers. *Rubber Chemistry and Technology*, **68**, 435–460.
- Lake, G. J. and Lindley, P. B. (1964). Cut growth and fatigue of rubbers. ii. experiments on a noncrystallizing rubber. *Journal of Applied Polymer Science*, **8**, 707–721.
- Le Cam, J.-B. (2005). *Endommagement en fatigue des elastomères*. Ph.d. thesis, Université de Nantes, École Centrale de Nantes.
- Le Cam, J.-B. (2017). Energy storage due to strain-induced crystallization in natural rubber: The physical origin of the mechanical hysteresis. *Polymer*, **127**, 166 – 173.
- Le Cam, J.-B. and Toussaint, E. (2010). The mechanism of fatigue crack growth in rubbers under severe loading: the effect of stress-induced crystallization. *Macromolecules*, **43**, 4708–4714.
- Le Cam, J.-B., Huneau, B., Verron, E., and Gornet, L. (2004). Mechanism of fatigue crack growth in carbon black filled natural rubber. *Macromolecules*, **37**, 5011–5017.
- Le Cam, J.-B., Verron, E., and Huneau, B. (2008). Description of fatigue damage in carbon black filled natural rubber. *Fatigue and Fracture of Engineering Materials & Structures*, **31**, 1031–1038.
- Le Cam, J.-B., Huneau, B., and Verron, E. (2013). Fatigue damage in carbon black filled natural rubber under uni- and multiaxial loading conditions. *International Journal of Fatigue*, **52**, 82 – 94.
- Le Cam, J.-B., Huneau, B., and Verron, E. (2014). Failure analysis of carbon black filled styrene butadiene rubber under fatigue loading conditions. *Plastics, Rubber and Composites*, **43**, 187–191.
- Le Chenadec, Y. (2008). *Autoéchauffement, fatigue thermomécanique des élastomères*. Ph.d. thesis, Ecole Polytechnique X.
- Le Saux, V. (2010). *Fatigue and ageing of rubbers under marine and thermal*

- environments: from accelerated tests to structure numerical simulations*. Ph.d. thesis, Université de Bretagne Occidentale - Brest.
- Legorju-Jago, K. and Bathias, C. (2002). Fatigue initiation and propagation in natural and synthetic rubbers. *International Journal of Fatigue*, **24**, 85–92.
- Lindley, P. (1974). Non-relaxing crack growth and fatigue in a non-crystallizing rubber. *Rubber Chemistry and Technology*, **47**, 1253–1264.
- Lu, C. (1991). *Etude du comportement mécanique et des mécanismes d'endommagement des élastomères en fatigue et en fissuration par fatigue*. Ph.d. thesis, Conservatoire National des Arts et Métiers.
- Mars, W. V. (2001). *Multiaxial fatigue of rubber*. Ph.d. thesis, PhD. University of Toledo.
- Mars, W. V. and Fatemi, A. (2002). A literature survey on fatigue analysis approaches for rubber. *International Journal of Fatigue*, **24**, 949–961.
- Masquelier, I. (2014). *Influence of formulation on the fatigue properties of elastomeric materials*. Ph.d. thesis, Université de Bretagne Occidentale.
- Moon, S.-I., Cho, I.-J., Woo, C.-S., and Kim, W.-D. (2011). Study on determination of durability analysis process and fatigue damage parameter for rubber component. *Journal of mechanical science and technology*, **25**, 1159–1165.
- Muñoz-Mejia, L. (2011). *Étude expérimentale des mécanismes d'endommagement par fatigue dans les élastomères renforcés*. Ph.d. thesis, Université Claude Bernard Lyon 1.
- Neuhaus, C., Lion, A., Jöhrlitz, M., Heuler, P., Barkhoff, M., and Duisen, F. (2017). Fatigue behaviour of an elastomer under consideration of ageing effects. *International Journal of Fatigue*, **104**, 72 – 80.
- Oshima, H., Noguchi, H., Shibata, S., Ochi, K., and Aono, Y. (2007). Fatigue characteristics of vulcanized natural rubber for automotive engine mounting. In *Progresses in Fracture and Strength of Materials and Structures*, volume 353 of *Key Engineering Materials*, pages 178–181. Trans Tech Publications.
- Ostojka-Kuczynski, E. (2005). *Comportement en fatigue des élastomères : application aux structures antivibratoires pour l'automobile*. Ph.d. thesis, École Centrale de Nantes.
- Ostojka-Kuczynski, E., Charrier, P., Verron, E., Marckmann, G., Gornet, L., and Chagnon, G. (2003). Crack initiation in filled natural rubber: experimental database and macroscopic observations. In J. J. C. Busfield and A. Muhr, editors, *Constitutive Models for Rubber III*, pages 3–10. Balkema.
- Poisson, J.-L. (2012). *Détermination d'un critère de fatigue multiaxial appliqué à un élastomère synthétique*. Ph.d. thesis, Université François Rabelais de Tours.
- Raoult, I. (2005). *Elastomeric structures upon cyclic loading : mechanical behaviour, fatigue, lifetime*. Ph.d. thesis, Ecole Polytechnique X.
- Roberts, B. J. and Benzies, J. B. (1977). The relationship between uniaxial and equibiaxial fatigue in gum and carbon black filled vulcanizates. **2**, 1–13.

- Robisson, A. (2000). *Comportement mécanique d'un élastomère chargé en silice. Etude de l'influence des charges et modélisation par une loi visco-hyperélastique endommageable*. Ph.d. thesis, Ecole des Mines de Paris.
- Ruellan, B., Le Cam, J.-B., Robin, E., Jeanneau, I., Canévet, F., Mauvoisin, G., and Loison, D. (2018). Fatigue crack growth in natural rubber: the role of strain-induced crystallization investigated through post-mortem analysis of fatigue striations. *Submitted in Engineering Fracture Mechanics*.
- Saintier, N. (2000). *Prévisions de la durée de vie en fatigue du NR, sous chargement multiaxial*. Ph.d. thesis, École Nationale Supérieure des Mines de Paris.
- Samaca Martinez, J. R., Le Cam, J.-B., Balandraud, X., Toussaint, E., and Cail- lard, J. (2013). Thermal and calorimetric effects accompanying the deformation of natural rubber. part 2: quantitative calorimetric analysis. *Polymer*, **54**, 2727 – 2736.
- Shangguan, W.-B., feng Zheng, G., Liu, T.-K., Duan, X.-C., and Rakheja, S. (2017). Prediction of fatigue life of rubber mounts using stress-based damage indexes. *Proceedings of the Institution of Mechanical Engineers, Part L: Journal of Materials: Design and Applications*, **231**, 657–673.
- Svensson, S. (1981). Testing methods for fatigue properties of rubber materials and vibration isolators. *Polymer Testing*, **2**, 161–174.
- Trabelsi, S. (2002). *Etude statique et dynamique de la cristallisation des élastomères sous tension*. Ph.d. thesis, Université Paris XI Orsay.
- Trabelsi, S., Albouy, P.-A., and Rault, J. (2002). Stress-induced crystallization around a crack tip in natural rubber. *Macromolecules*, **35**, 10054–10061.
- Treloar, L. R. G. (1975). *The Physics of Rubber Elasticity*. Oxford University Press, Oxford.
- Wang, X.-L., Shangguan, W.-B., Rakheja, S., Li, W.-C., and Yu, B. (2014). A method to develop a unified fatigue life prediction model for filled natural rubbers under uniaxial loads. *Fatigue & Fracture of Engineering Materials & Structures*, **37**, 50–61.
- Woo, C.-S., Kim, W.-D., Lee, S.-H., Choi, B.-I., and Park, H.-S. (2009). Fatigue life prediction of vulcanized natural rubber subjected to heat-aging. *Procedia Engineering*, **1**, 9–12.
- Wöhler, A. (1860). Versuche über die festigkeit eisenbahnwagenachsen. *Z Bauwesen*, **10**.
- Xie, J. (1992). *Etude de la fatigue et de la rupture des assemblages collés composite-élastomère*. Ph.d. thesis, Ecole Centrale de Paris.
- Zarrin-Ghalami, T. and Fatemi, A. (2013). Multiaxial fatigue and life prediction of elastomeric components. *International Journal of Fatigue*, **55**, 92 – 101.